On the use of supersonic particle deposition to restore the structural integrity of damaged aircraft structures

R. Jones [a,*], N. Matthews [b], C.A. Rodopoulos [a], K. Cairns [a], S. Pitt [a]

[a] DSTO Centre of Expertise in Structural Mechanics, Department of Mechanical and Aeronautical Engineering, PO Box 31, Monash University, VIC 3800, Australia
[b] Rosebank Engineering, 836 Mountain Highway, Bayswater, VIC 315, Australia

ARTICLE INFO

ABSTRACT

The paper presents a preliminary experimental study and an analysis of the potential application of supersonic particle deposition (SPD) for repairing and restoring the airworthiness and functionality of aging aircraft structures. In this work the fatigue performances of cracked metallic structures with a SPD doubler/patch under constant amplitude loading were monitored using infra-red thermography, whereas for the baseline specimen test the crack length was monitored using digital cameras. In all the cases the experimental data revealed that the baseline specimens, i.e. without an SPD patch, accrued damage more rapidly and that crack growth was significantly greater than the corresponding SPD patched panels. In the majority of tests cases the patched panels showed little evidence of damage/crack growth. A prediction of the fatigue performance of an SPD patched single edge notch coupon is made using SIF values calculated via an approximate analysis and the resultant crack length history is in good agreement with experimental data. Weight function solutions for SPD repairs to centre cracked panels are also developed and validated via three dimensional finite element analysis. The paper concludes that SPD is effective in containing damage and that the proposed analytical solution is good first approximation that can be used to calculate the associated SIF and thereby account for the effect of an SPD patch on crack growth.

1. Introduction

The significance of this research is evident from the June 2007 Report to Congress by the Under Secretary of the Department of Defence (Acquisition, Technology and Logistics) [1]. This report estimated the cost of corrosion associated with US DoD systems to be between $10 billion and $20 billion annually. To address this problem Section 1067 of the Bob Stump National Defense Authorization Act, US Congress Public Law 107-3 14 (NDAA) requires the Secretary of Defense to designate an official or organization to be responsible for the prevention and mitigation of corrosion of military equipment and infrastructure. It also requires the development and implementation of a long-term strategy. As a result of a subsequent detailed study of the problem of corrosion the US DoD has focused its life-cycle corrosion research and development efforts on four primary areas [1]. One of these four areas is: Repair processes that restore corroded materials to an acceptable level of structural integrity and functionality. This topic is one of the focal points of the present paper.

To meet this challenge this paper evaluates the potential for supersonic particle deposition (SPD) technology [2–7] to be used

to restore the structural integrity of damaged aluminium alloy structural components. This process was developed in Russia in the 1980s at the Institute for Theoretical and Applied Mechanics in Novosibirsk. The SPD process is currently mainly used to deposit metal, alloy, polymer, or composite powder material onto a substrate to provide a protective coating and in some instances to restore damaged/worn geometries, see Figs. 1 and 2. The coating is formed by exposing the structure/component to high velocity (typically between 300 and 1200 m/s) solid-phase particles, which have been accelerated by a supersonic gas flow, usually either nitrogen or helium, at a temperature that can range between 400 and 900 °C. When used to protect aluminium alloys from corrosion it usually involves the deposition of a pure aluminium surface layer/coating.

It should be stressed that, to date, SPD has primarily been used to produce protective coatings [2–7]. More recent aerospace applications have seen SPD being used to restore damaged/worn geometry [7–10]. In this context a joint US Army/US Navy study [7] has shown how this technology can be used to protect magnesium helicopter components and [9] outlines how the technique is now widely used to rehabilitate damaged/worn components on Royal Australian Navy helicopters. However, little attention has been given to using this technique to restore the damage tolerance of damaged aluminium alloy aerospace components, which is the

As-sprayed repair of the lip of helicopter magnesium housing

As-sprayed aluminium-Al203 repair of Al-Si 356 cast engine block

Fig. 1. Examples of geometry restoration using SPD, from [8].

Fig. 2. Rosebank Engineering Restoration of a Seahawk Helicopter Main Gear Box Module Aft Flight Control Pad, from [9].

focal point of this paper. As a result of this study it would appear that this process has the potential to be a viable alternative to the use of externally bonded composite repairs [11,12] for extending the fatigue life of damaged structural components. Indeed, this process has recently been approved by the Directorate General Technical Airworthiness for application to RAAF and Australian Navy aircraft. As such there is an urgent need to address damage tolerance issues. This topic is the focal point of the present paper.

To this end this paper presents the results of a series of laboratory tests on 2024-T3 and 7050-T7451 single edge notch tension panels (SENT) repaired using SPD patches where it is shown that SPD patches can significantly increase the fatigue life and that the fractal box dimension D of failed SPD surfaces was approximately 1.5. In the case of the 7050-T7451 SENT panel it is shown that crack growth in the panel can be reasonably accurately computed by assuming that the reduction in the stress intensity factor is (only) due to the reduction in the net section stress.

A weight function solution for centre cracked panels repaired using SPD subjected to an arbitrary stress field is also presented and the solution validated via three dimensional finite element analysis.

2. Supersonic particle deposition

To study the effect of a supersonic particle deposition (SPD) on the fatigue performance of cracked metallic structures initial tests were performed on a 350 mm long and 1.27 mm thick 2024-T3 clad aluminium alloy dogbone specimen which contained a centrally located 2 mm long edge notch, see Figs. 3–5.

These initial tests were performed under constant amplitude loading with $\sigma_{max} = 181$ MPa and $R = \sigma_{min}/\sigma_{max} = 0.1$. (This stress level was chosen since it represents a realistically upper bound on stresses that can be expected in a thin (1 mm) wing skin.) Two specimens were tested, one without a SPD doubler, and one with a 1 mm thick full width doubler, that extended over the working section of the specimen, deposited on either side of the specimen, see Figs. 4 and 5. The doublers were deposited at Rosebank Engineering using a 7075 Aluminium Alloy powder with a nominal particle size of between 30 and 40 μm and the Rosebank propriety deposition process, which has been specifically developed for depositing aluminium alloy powders.

For the baseline specimen test the crack length was monitored using digital cameras. However, whilst there are numerous non-destructive inspection tools that are commonly used to monitor crack growth in aircraft structures, i.e. ultrasonics, eddy currents, thermography, etc., the present study used Lock-in infra-red thermography to simultaneously monitor the evolution of the stress and the damage states in the 2024-T3 skin and the SPD doublers. (At this point it should be noted that to ensure a uniform emissivity the surface being monitored was sprayed matt black and that thermography was used as a qualitative rather a quantitative measure of the stresses and the fatigue damage. Details on the use of
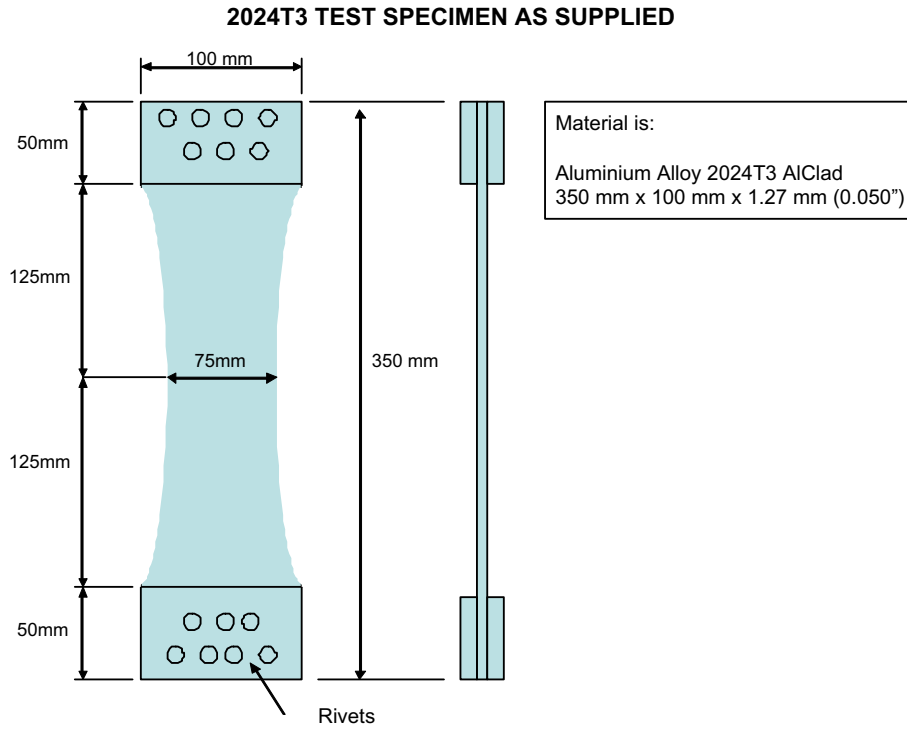
2024T3 TEST SPECIMEN AS SUPPLIED

Fig. 3. Geometry of the edge notch panel.
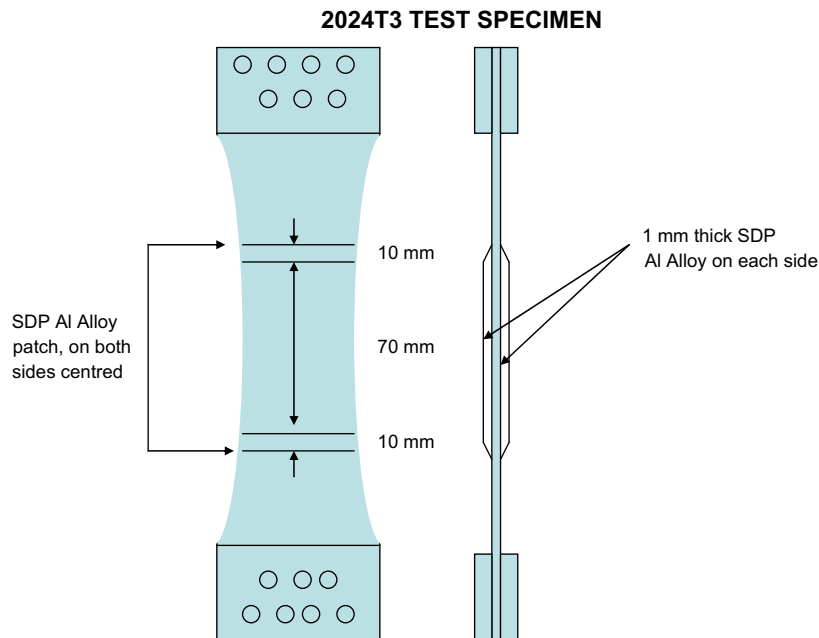
2024T3 TEST SPECIMEN

Fig. 4. Geometry of the panel and the SPD doubler.

Lock-in thermography to measure surface stresses and energy dissipation are given in [13–15].) The baseline specimen, i.e. without a doubler, lasted approximately 35,000 cycles. In contrast the 7075 SPD patched panel test was stopped after approximately 60,000 cycles with little, i.e. no evident, damage in the 7075 SPD or crack growth in the 2024-T3 skin. Figs. 6 and 7 present infrared pictures of the stress field at 11,100 and 56,100 cycles respectively. These figures show that the stresses in the SPD doubler remained essentially unchanged throughout the test.

2.1. Single edge notch tension (SENT) SPD strip tests

To further study the ability of SPD doublers to reduce crack growth tests were performed on a single edge notch dogbone specimen, with a geometry as described above and an (initial) 1.4 mm long edge notch. In the initial base line test there was no SPD and the specimen was tested under constant amplitude loading with a peak stress in the working section of σ_{max} = 93.36 MPa and R ($\sigma_{min}/\sigma_{max}$) = 0.1. This stress level was chosen to represent a typical
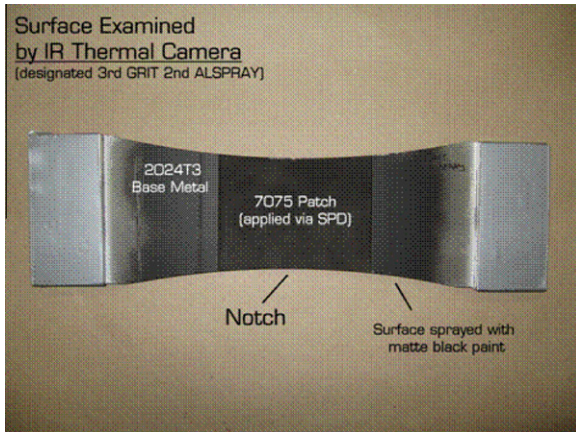
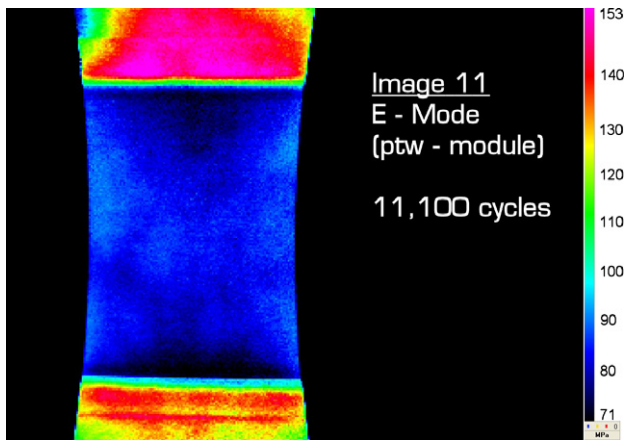Fig. 5. Plan view of the test panel and the SPD doubler.

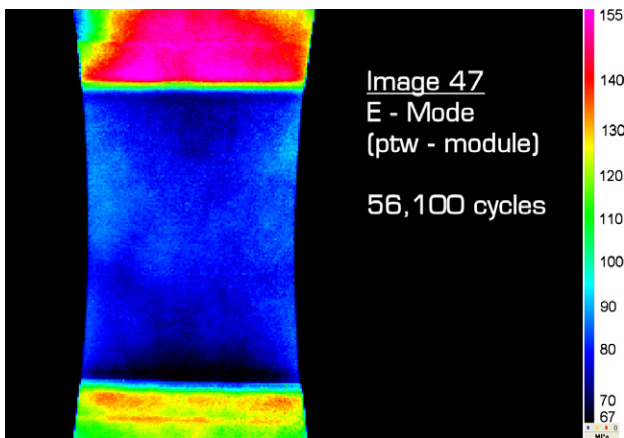Fig. 6. Stresses in the SPD doubler at 11,100 cycles, units are in MPa.

Fig. 7. Stresses in the SPD doubler at 56,100 cycles, units are in MPa.

Fig. 8. Crack growth histories in the SENT tests.

fuselage skin stress. Crack growth in the 2024-T3 plate was monitored using digital cameras and the resultant crack length versus cycles history is shown in Fig. 8.

In the next test, the specimen was first loaded so as to grow a sharp crack. This first phase of the test was stopped at 18,886 cycles when the crack length was approximately 3.2 mm. A 10 mm wide and 1 mm thick SPD strip with a nominally (isosceles) triangular crosssection, see Figs. 9 and 10, was then installed and the test was continued. The Crack growth in the 2024-T3 plate was again
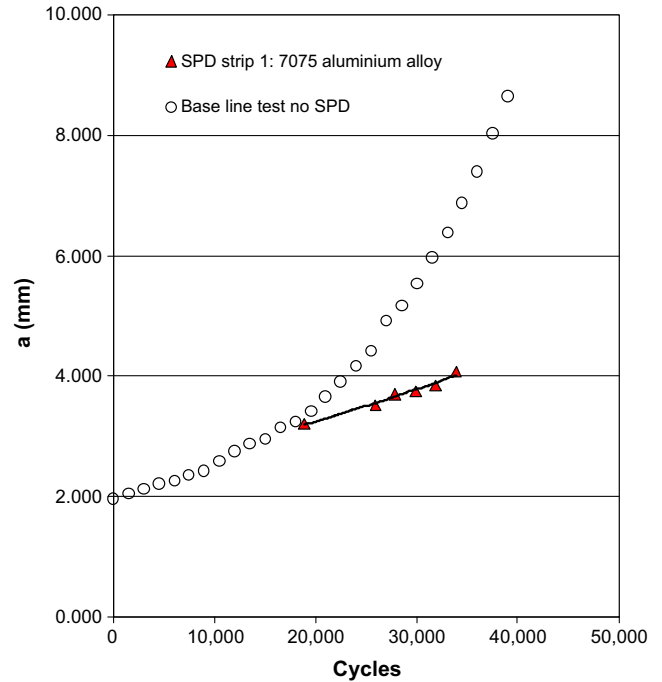
monitored using digital cameras whilst the stress field in both the SPD strip and the 2024-T3 skin and the degradation in the SPD strip was monitored using Lock-in infrared themography.

An infrared stress image captured shortly after the restart of the test is shown in Fig. 11. In this figure the picture was captured at a cyclic stress amplitude $\Delta\sigma$, remote from the centre line of the specimen, of approximately 53 MPa. This was done so as to not overly influence crack growth in the skin. Here we see how the stress field in the SPD ahead of the crack is contiguous with that in the plate, i.e. the SPD is taking load in the region ahead of the crack. We also see hot spots in the skin outboard of the ends of the SPD strip which establish that the SPD strip was indeed pulling load from the skin. This is essential if the process is to enhance the damage tolerance of the skin. The resultant crack growth data is shown in Fig. 8 where we see that the use of a 7075 aluminium alloy SPD strip has significantly reduced the crack growth rate.

A second test was then performed whereby the SPD strip was applied to a 0.3 mm long initial edm[1] crack (notch) where the crack was not sharpened (grown) prior to installation of the SPD strip. In this case the test was stopped after approximately 345,000 cycles since there was no apparent crack growth at the notch (crack) or damage in the SPD.

2.2. Cracking in 7050-T7451 SENT tests

It is well known that for combat aircraft most of the fatigue life of the structure is consumed in the growth of short cracks [16]. Consequently to evaluate the effect of a SPD repair on small flaws in aircraft structural components we tested a 3 mm thick SENT (single edge notch tension) dogbone specimen, with a $K_t = 1.11$, with a thin 0.5 mm thick 7075 aluminium alloy SPD patch on one side. The 7050-T7451 specimen was 350 mm long, 42 mm wide and 3 mm thick and had a 0.69 mm radius semi-circular edge notch on one side. The specimen was tested at a peak stress, in the working section, of 140.0 MPa with $R = 0.1$. This corresponds to a
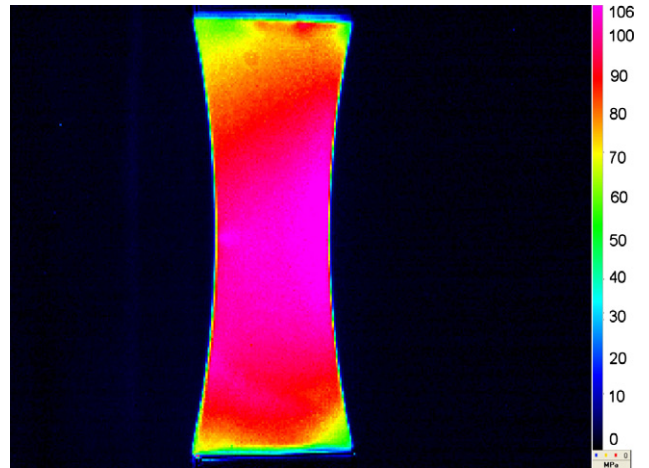
_____

[1] Electrical discharge machined (edm).
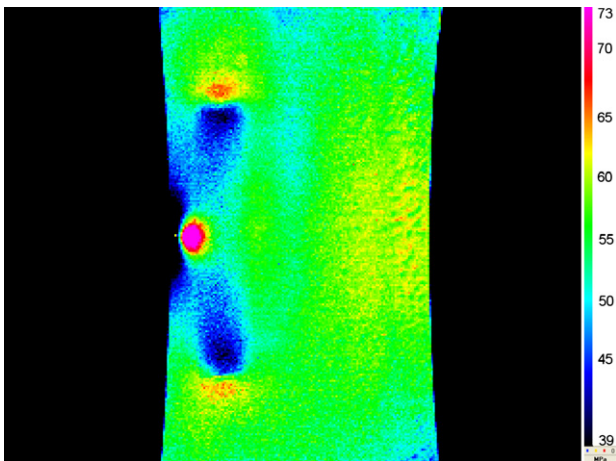
2024T3 TEST SPECIMEN WITH SPD REPAIR
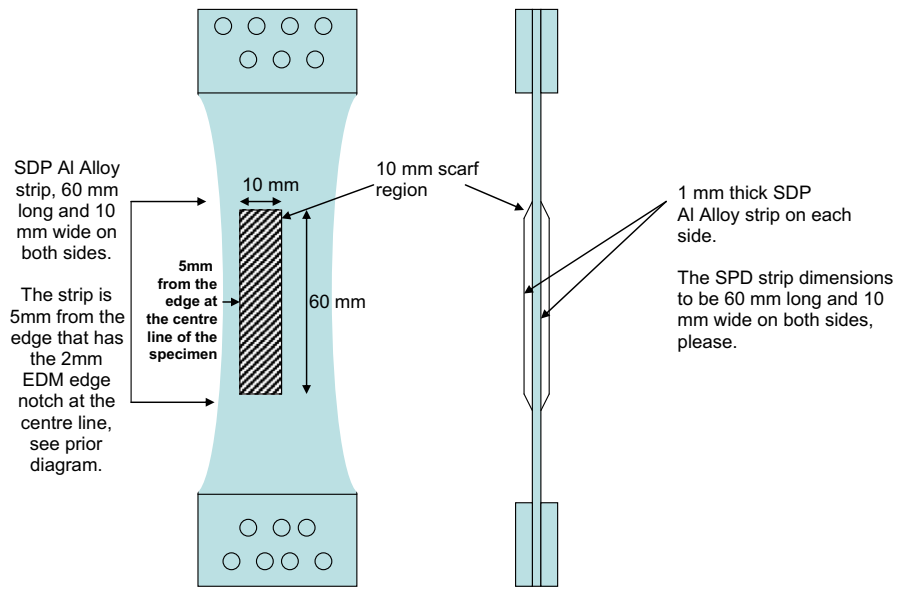
Fig. 9. Schematic diagram showing the location of the SPD strip.

Fig. 10. View showing the crossection of the SPD strip.

Fig. 11. The stress field in the skin and the SPD strip, units are in MPa.

peak (remote) load of 17.64 kN with R = 0.1 and was chosen to represent the stress, at limit load, in the wing skin of a typical fighter aircraft.

Fig. 12. Stresses in the SPD at 3000 cycles, units are in MPa.

A thin SPD doubler was used so that, in this test program, we could evaluate the damage induced, as the crack opened and closed during fatigue loading, in the interfacial region between the SPD and the 7050-T7451. This damage could have been reduced by increasing the thickness of the SPD thereby lowering the stresses in the underlying 7050-T7451 and subsequently reducing the opening of the crack.

The ability of the SPD doubler to pull load from the underlying 7050-T7451 structure is clear from the E-Mode (stress) Lockin thermography picture of the stresses on the specimen side with the SPD patch at 3000 cycles, see Fig. 12. Although the crack in the 7050-T7451 specimen was not immediately evident an analysis of the infra-red data associated with the left hand side of the specimen shown in this picture, i.e. in the SPD directly over the crack, revealed an indication of the crack under the patch. After 33,000 cycles the crack in the 7050-T7451 had grown to a length of approximately 4.2 mm and the resultant stress picture is shown in Fig. 13. At this point we now see evidence of delamination damage (disbonding) on the LHS of the SPD in the region that lay over the crack.
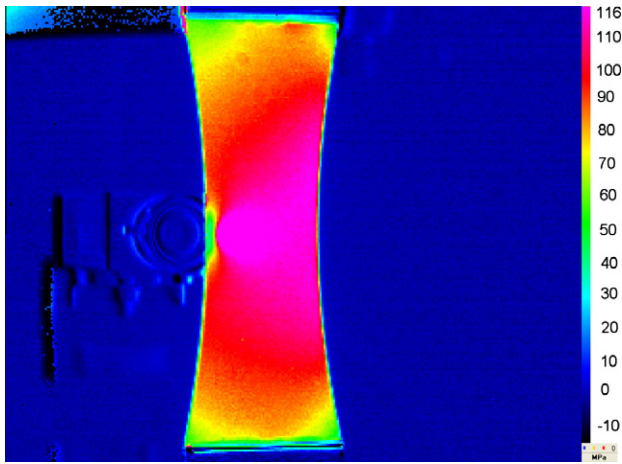
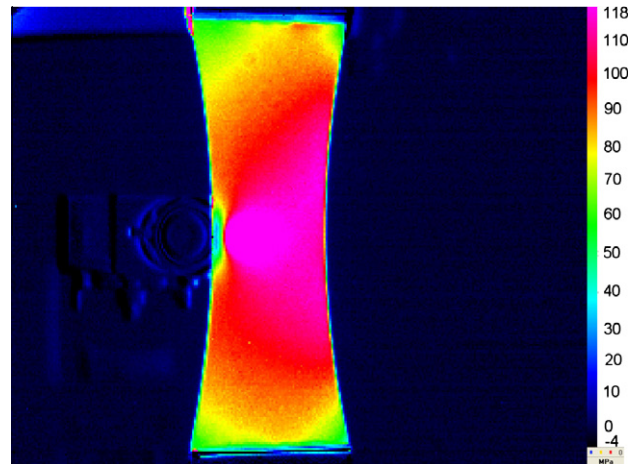Fig. 13. Stresses in the SPD at 33,000 cycles, units are in MPa.

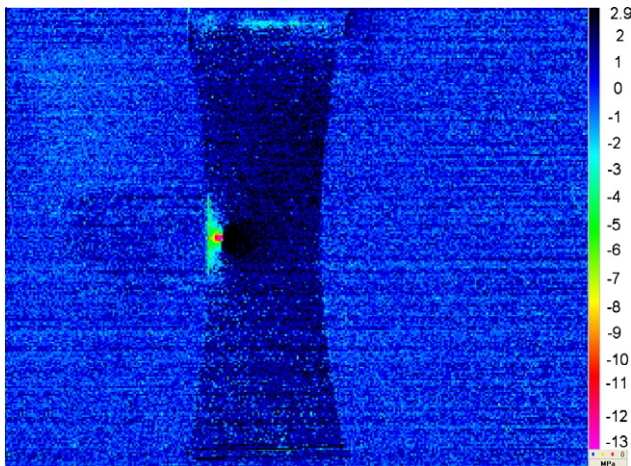Fig. 15. Stresses in the SPD at 35,500 cycles, units are in MPa.

Fig. 14. Dissipated energy at 33,500 cycles, units are in MPa.
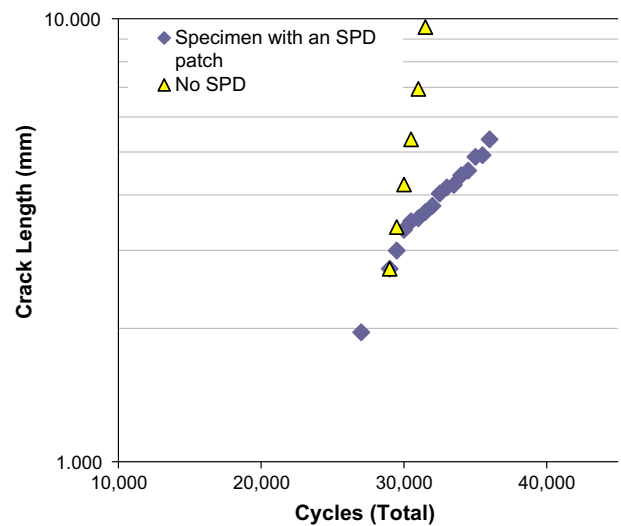

Fig. 16. Measured crack length histories with and without an SPD patch.

The extent of the damage is illustrated in Fig. 14 which presents a picture of the dissipated energy at 33,500 cycles. (Note that the dissipated energy associated with the crack tip is clearly evident in this figure. This is important because it raises the potential of non-destructive inspection of the specimen through the SPD doubler.) At 35,500 cycles the crack had grown to approximately 4.92 mm and the associated stress picture is shown in Fig. 15 where we can see that the delamination in the SPD has grown slightly.

It would thus appear that whilst damage to the SPD interface can result due to crack opening the onset of damage does not appear to lead to immediate (catastrophic) failure in the SPD. As such damage growth in the SPD can be included in the damage tolerance assessment of the SPD repair process. Furthermore, given that there was no apparent damage at the ends of the SPD the damage in the central region over the crack can be controlled by increasing the thickness of the SPD in this region thereby reducing the stress in the 7050-T7541 together with the associated crack opening displacement.

The test was stopped at 37,000 cycles at which stage the crack was approximately 5.3 mm long. A plot of the measured crack length versus cycles history is presented in Fig. 16 together with test data for the case when there was no SPD. Here we see that the SPD patch has somewhat reduced the crack growth rate.

To further confirm the ability of SPD to restore structural integrity and to illustrate the ability to control the onset of delamination damage over the crack a test was subsequently performed on a 1 mm thick 7050-T7451 SENT specimen, with a 0.8 mm long initial edge crack and an in-plane geometry as per the previous test. This specimen had two 0.5 mm thick SPD doublers on either side of the specimen. The specimen was subjected to a peak (remote) load of 5.88 kN with $R = 0.1$ which equates to the same remote stress as in the previous test. In this case the test was stopped after 117,000 cycles as there was no apparent crack growth and no apparent degradation in the SPD.

3. Predicting crack growth in the 7050-t7451 sent test

Let us now attempt to predict the crack length history seen in the 7050-T7451 SENT test outlined in Section 2.2. Here we tested a 3 mm thick SENT (single edge notch tension) dogbone specimen with a thin 0.5 mm thick 7075 aluminium alloy SPD patch on one side. The specimen was 350 mm long, 42 mm wide and 3 mm thick and had a 0.69 mm radius semi-circular edge notch on one side. The specimen was subjected to a peak (remote) load of 17.64 kN with $R = 0.1$.

The stress intensity factor for a through-the-thickness crack of length c emanating from the centre of the notch of radius r is given in [17] as:
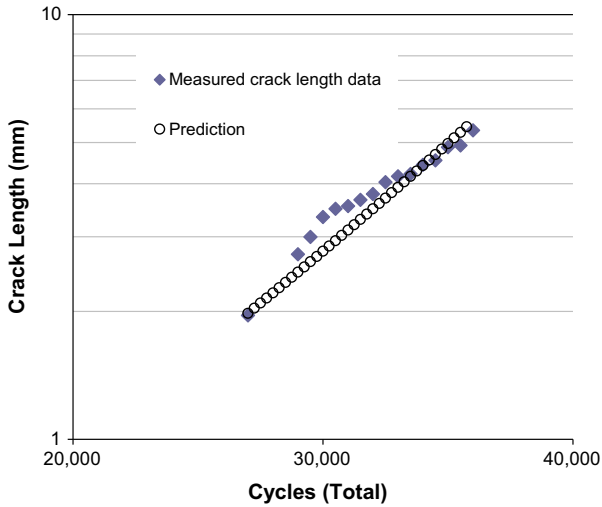
Fig. 17. Measured and predicted crack length histories for the SENT specimen with an SPD patch.

$$K = f_1 g_4 f_w \sigma \sqrt{(\pi c)} \qquad (1)$$

where c is the length of the crack emanating from the notch and σ is the stress in the 7050-T7451 underneath the SPD. The values of f_1, g_4 and f_w, taken from [17], are:

$$f_1 = 1 + 0.358\varphi + 1.425\varphi^2 - 1.578\varphi^3 + 2.156\varphi^4 \qquad (2)$$

$$\varphi = 1/(1 + c/r) \qquad (3)$$

$$g_4 = K_t(0.36 - 0.32/\sqrt{(1 + c/r)}) \qquad (4)$$

$$f_w = 1 + 2.7\varphi^2 - 3.5\varphi^4 + 3.8\varphi^6 \qquad (5)$$

$$K_t = 3.17 \qquad (6)$$

Since the specimen was tested using hydraulic grips the formulae used for f_w was the fixed displacement expression given in [17].

Let us now attempt to use this solution to predict crack growth. Fig. 13–15 revealed that there was (delamination) damage growth in the SPD over the crack. Thus as recommended in [18] for composite repairs to cracked metal skins we analysed the problem by assuming that the resultant stress intensity factor was equal to the solution to the SENT specimen subjected to a stress field σ_o which corresponds to the stress in the (base) specimen under the SPD in the absence of a crack.

The DSTO Combat and Trainer Aircraft Group [19–21] have shown that the growth of small flaws in 7050-T7451 conforms to the Generalised Frost-Dugdale crack growth law, viz:

$$da/dN = C^* a^{(1-\gamma/2)} (\Delta K^{(1-p)} K_{max} p / \sigma_y)^\gamma / (1 - K_{max}/K_c) \qquad (7)$$

where C_*, γ and K_c are material constants and a, K_{max} and ΔK are crack lengths, the maximum value of the stress intensity factor at cycle N and the range of the stress intensity factor at cycle N respectively. The crack length history was predicted by integrating Eq. (7) using Eqs. (1)–(8) with P_{max} = 17.4 kN, R = 0.1 and r = 0.69 mm. In this calculation we took the values of γ, p, C_*, σ_y to be as given in [19,21], viz: γ = 3, p = 0.2, C_* = 0.50, σ_y = 460 MPa and, for this thickness, $K_c \sim$ 50–65 MPa $\sqrt{}$m. (In this analysis we used a value of K_c = 60 MPa $\sqrt{}$m. However, for this range of loads and crack lengths the value has a small effect on the crack length predictions.) The resultant predicted crack length history is shown in Fig. 17 where we see a reasonably good agreement between the measured and predicted crack length histories.

It would thus appear that, in this case, as for cracks growing under composite repairs [18] the stress intensity factor can be approximated as the solution to the SENT specimen subjected to the stress field σ_o which corresponds to the stress in the (base) specimen under the SPD in the absence of a crack. One advantage of this approach is that the computed crack length history should be conservative.

4. Approximate solutions for centre cracked panels repaired using spd

In the previous section we considered the case of a thin (0.5 mm) SPD repair to a small flaw in a relatively thick (3 mm) section and we saw that the SPD delaminated on either side of the crack. In such cases it was reasonable to assume that the dominant effect of the SPD was to merely reduce the net section stress [18]. However, for certification purposes we need the solution for the stress intensity factor associated with an arbitrary length crack where SPD patch is not thin. We also need to establish if, for a given crack length, the stress intensity factor range ΔK is beneath the threshold value ΔK_{th} as this will significantly simplify the certification process. To this end this paper will consider an SPD repair of thickness t_r to a centre cracked panel, thickness t_p, with an interfacial region, thickness t_i, that has been (potentially) affected by the SPD process subjected to a remote stress σ as shown in Fig. 18.

The SPD process can result in an interfacial region that has been affected by the SPD process [22–24]. For the aluminium alloy powders used in SPD repairs the maximum particle size is approximately 40 μm. Consequently the thickness (t_i) of this region is generally very small [22–24] in comparison to the thickness of the underlying plate, i.e. typically less than 0.1–0.15 mm, see Fig. 19. As a result this problem is analogous to that of a bonded repair where the interfacial region mimics the adhesive that joins the repair to the plate. It is known that for small cracks in metal skins repaired using a composite patch the 2D solution for the stress intensity factor is essentially due to the reduction in the stress field under the repair whilst for long cracks the stress intensity factor asymptotes to a limiting stress intensity factor K_∞ as the crack length increases, see [18,25–28]. As such it follows that the 2D solution for the stress intensity factor associated with small cracks repaired using SPD is also essentially due to the reduction in the stress field under the SPD whilst for long cracks repaired using SPD the stress intensity factor should also asymptote to a
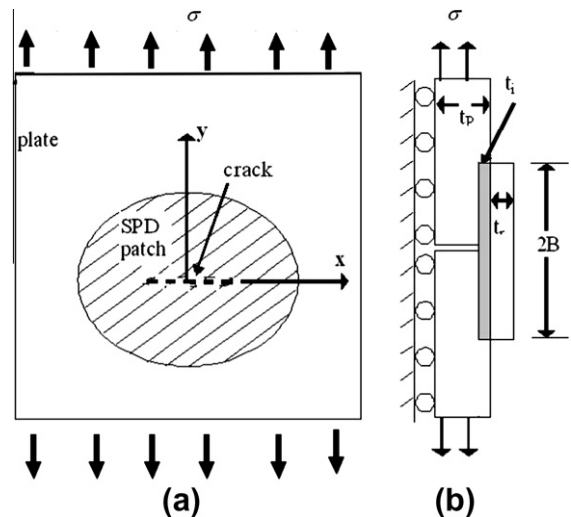

Fig. 18. Repair configuration: (a) plan view, (b) cross-section along centre line, i.e. x = 0.
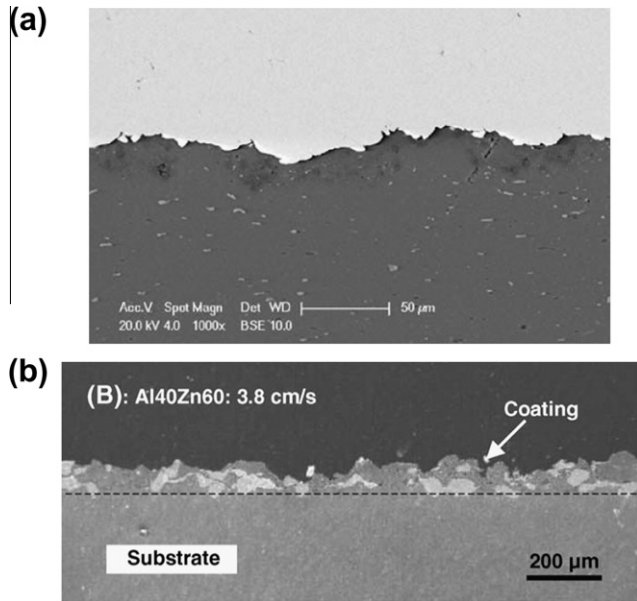
Fig. 19. (a) Images of Cu (bright) on an Al substrate, from [22], and (b) AlZn onto an Al substrate, from [23].

limiting stress intensity factor K_∞ as the crack length increases. The approximate formulae for this asymptote thus follows from [26], see pp. 216–218, viz:

$$K_\infty = Y\Omega_L \sigma_0 \sqrt{\pi a} \tag{8}$$

where

$$\sigma_0 = \sigma E_p t_p / (E_p t_p + E_r t_r) \tag{9}$$

Y is a geometry factor, = 1 for a large centre cracked panel and Ω_L is a load attraction factor that accounts for the different stiffness of the repaired region. (In this paper we will take $\Omega_L = 1$.) The term $\pi\lambda$ is given by the expression

$$\pi\lambda = \sqrt{E_p t_p / \beta(1 + t_p E_p / E_r t_r)} \tag{10}$$

where

$$\beta = (t_i/G_i + t_r/3G_r + t_p/3G_p)/(t_i/G_i + 3t_r/8G_r + 3t_p/8G_p)^2 \tag{11}$$

Here t_i, t_p and t_r are the thickness' of the interface region where, the SPD has modified the properties of the plate, of the plate, and of the SPD respectively, G and E denote the shear and Young's modulus and the subscripts i, p and r denote their values for the interfacial bonding region, the plate, and the SPD repair respectively. (The notation used in this section follows that given in [26] pp. 217–218.) This expression, i.e. Eq. (11), is an extension of the formulae first developed in [25] in that it allows for the interfacial thickness t_i to be negligible. This (allowance) is important since for SPD repairs the modulii of each region will generally be comparable and the interfacial thickness t_i that is affected by the SPD process is expected to be very small. As such the terms in Eq. (11) related to the term t_i/G_i are small in comparison with those terms relating to the SPD repair ($t_r/3G_r$) and the plate ($t_p/3G_p$). Consequently the expression for β can often be approximated as:

$$\beta = (t_r/3G_r + t_p/3G_p)/(3t_r/8G_r + 3t_p/8G_p)^2 \tag{12}$$

It is expected that, in many instances, the SPD powder, used in the repair, and the plate material will have essentially the same modulii, i.e. aluminium plates are expected to be repaired using aluminium alloy powders and steel components are likely to be repaired using steel powders. In such cases we can approximate G_r by G_p so that Eq. (12) reduces to:
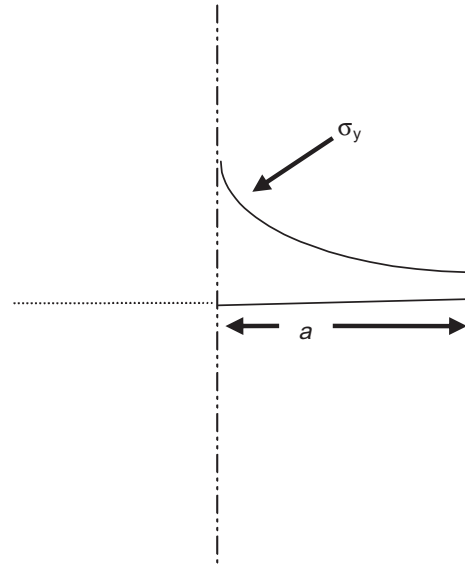

Fig. 20. Schematic picture showing the stresses used to determine K.

$$\beta = 64 G_p / 27(t_r + t_p) \tag{13}$$

Having established the asymptotic limit it follows from [28–30] that the functional form of K as a function of the crack length (a) can be approximated as:

$$K = W(a/\pi\lambda)\sigma_0\sqrt{(\pi a)} \tag{14}$$

where the function W, viz:

$$W(a/(\pi\lambda)) = \sqrt{[(1 + 2.23a/(\pi\lambda))/(1 + 3a/(\pi\lambda) + 7(a/(\pi\lambda))^2)]} \tag{15}$$

describes the transition from the small crack solution $a \to 0$ to the long crack solution $a \to \infty$, see [28,30] for more details[2]. Eqs. (14) and (15) reveal that for short cracks the reduction in the stress intensity factor is essentially due to the reduction in the stress in the plate due to the SPD patch, i.e.

$$\lim_{a \to 0} K = \sigma_0 \sqrt{\pi a} \tag{16}$$

For long cracks K tends to its asymptotic limit K_∞. In Eq. (14) we have used the functional form associated with [30] rather than that given in [28].

4.1. SPD repairs to cracks in an arbitrary stress field

Let us next consider the case of an SPD repair to a crack with a total of length $2a$ subjected to an arbitrary stress field. In this instance the solution for the stress intensity factor K follows from the above analogy with a composite repair to a crack in a metal skin under an arbitrary symmetry stress field [29], viz:

$$K = W(a/\pi\lambda)\underline{K} \tag{17}$$

where K is the solution to the entire cracked specimen subjected to a stress σ_0 which corresponds to the stress in the (base) specimen under the SPD in the absence of a crack is given by

$$\underline{K} = 2\sqrt{(a/\pi)} \int_0^a \sigma_y(x)/(a^2 - x^2)^{1/2} dx \tag{18}$$

and σ_y is the stress in the skin under the SPD in the absence of a crack, see Fig. 20.

---

[2] This functional form is a representation of the curve presented (graphically) in [30].
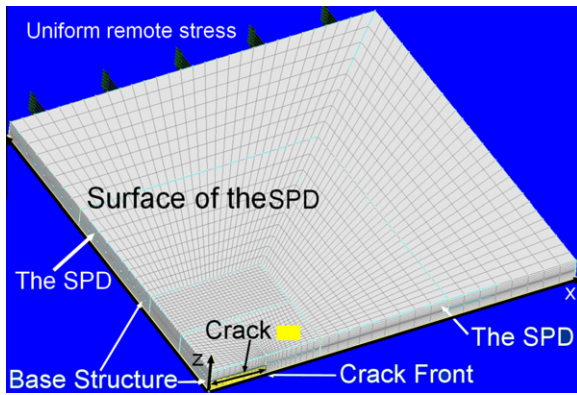
Fig. 21. A typical finite element mesh of the cracked structure and the associated SPD repair. The crack in the base structure (plate) is shown in a different colour to the SPD and the remainder of the cracked plate.

Fig. 22. Two SPD strips on either side of a 20 mm long central crack in a rib stiffened panel.

Table 1
Comparison between predicted and computed stress intensity factors.

a (mm)	Finite element $K_{\max}$ (MPa $\sqrt{m}$)	Analytical $K_{\max}$ (MPa $\sqrt{m}$)	Upper bound K_u (MPa $\sqrt{m}$)
1	4.88	5.03	5.60
3	6.77	6.82	9.71
5	7.29	7.29	12.53
10	7.56	7.59	17.72
15	7.60	7.65	21.71
20	7.60	7.68	25.07

Fig. 23. View of the delaminated surface of SPD strip (A), which was 20 mm wide, showing the locations where the fractal dimensions were measured.

To evaluate the accuracy of this approximation let us consider a 3 mm thick × 200 mm × 200 mm centre cracked plate repaired using a 3 mm (thick) × 200 mm × 200 mm SPD patch subjected to a remote uniform stress (in the skin) of 100 MPa. To this end three dimensional finite element models were constructed for: 2, 6, 10, 20, 30, and 40 mm long cracks. Due to symmetry considerations only one quarter of the structure needed to be modelled. In each case the models had approximately 66,000 three dimensional twenty-one nodded isoparametric brick elements and approximately 300,000 nodes, see Fig. 21. There were eight elements through the thickness of the SPD and eight elements through the thickness of the plate. In each case there were ten elements along the crack and the side length of the crack tip elements were approximately 1/100th of the length of the crack. The mid-side nodes associated with the near tip elements were moved to the quarter points so as to simulate the necessary $r^{-1/2}$ singularity. Bending of the SPD and the plate was prohibited. Both the aluminium alloy plate and the SPD were assumed to have a Young's modulus $E = 70{,}000$ MPa and a Poisson's ratio of 0.3.
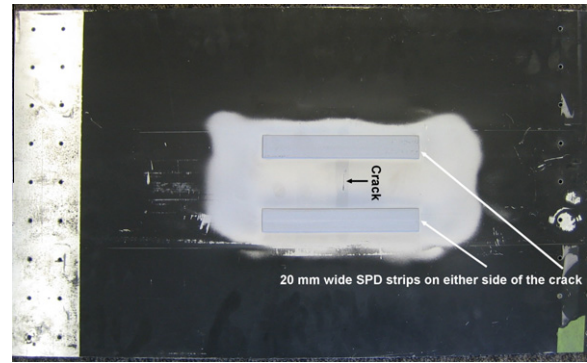
The computed values of the maximum value of the stress intensity factor $K_{\max}$ are given in Table 1 along with the associated analytical values, where Eq. (12) was used to compute β, and the quantity.

$$K_u = \sigma_o \sqrt{(\pi a)} \qquad (19)$$

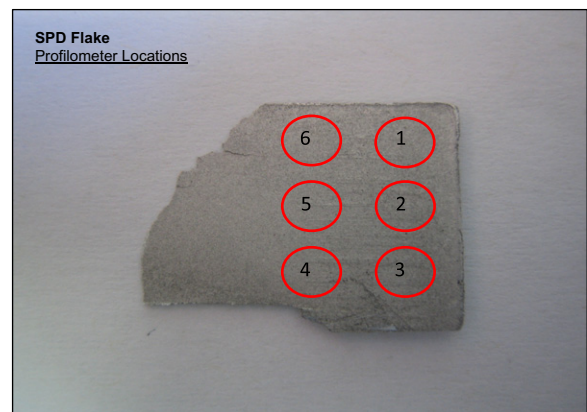which represents an upper bound on K. Here we see that the stress intensity factor associated with SPD repairs does indeed asymptote to a constant value and that this asymptote is in good agreement with the analytical approximation, i.e. Eq. (14).

5. Towards a quality control assessment tool

When performing composite repairs to aircraft structural members it is common practice to make travelling specimens that are subsequently used to assess the quality of the repair [11,12]. The challenge is to develop a similar approach for SPD modifications/repairs to aircraft structural components. As such this section raises the possibility of using simple specimens that are subsequently fatigue tested and the quality of the bond assessed via the fractal dimension [31] of the resultant fatigue surfaces.

In it this context it should be noted that is now known that fracture surfaces can be considered as a fractal set, see Mandelbrot et al. [31]. In this work Mandelbrot et al. [31] wrote:

"When a piece of metal is fractured either by tensile or impact loading the facture surface that is formed is rough and irregular. Its shape is affected by the metal's microstructure (such as grains, inclusions, and precipitates where characteristic length is large relative to the atomic scale), as well as by 'macrostructural' influences (such as the size, the shape of the specimen, and the notch from which the fracture begins). However, repeated observation at various magnifications also reveal a variety of additional structures that fall between 'micro' and 'macro' and have not yet been described satisfactorily in a systematic manner. The experiments reported here reveal the existence of broad and clearly distinct zone of intermediate scales in which the fracture is modelled very well by a fractal surface."

It is also known [32–34] that, prior to the onset of rapid fracture, fatigue crack surfaces in metals, that are not associated with very small crack lengths, have a fractal box dimension D, as defined in [32], that lies between approximately 1.2 and 1. Thus it may be possible to use this observation to quantify the quality of the SPD process. To do this travelling specimens would be fabricated in parallel with the SPD application. These travelling specimens would
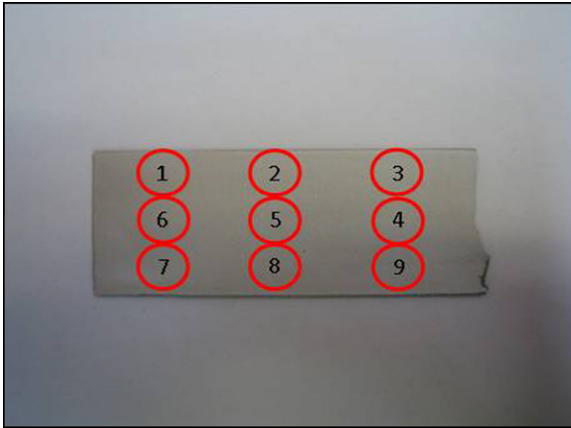
Fig. 24. View of the delaminated surface of SPD strip (B), which was 20 mm wide, showing the locations where the fractal dimensions were measured.

Table 2
Fractal box dimension (D) associated with the end of strip A.

	Random area 1 within location	Random area 2 within location
Loc 1	1.629	1.500
Loc 2	1.409	1.675
Loc 3	1.542	1.684
Loc 4	1.416	1.473
Loc 5	1.543	1.530
Loc 6	1.399	1.529
Average	1.49	1.57

Table 3
Fractal box dimension (D) associated with the end of strip B.

	Random area 1 within location	Random area 2 within location
Loc 1	1.673	1.613
Loc 2	1.482	1.521
Loc 3	1.525	1.614
Loc 4	1.551	1.49
Loc 5	1.526	1.516
Loc 6	1.558	1.561
Loc 7	1.578	1.482
Loc 8	1.503	1.593
Loc 9	1.584	1.563
Average	1.553	1.550

subsequently be fatigue tested and the associated fractal box dimensions measured. It is hypothesised that if D had a value that was near 1.2, or lower, then you would have a process that produced a fatigue crack surface that was consistent with that associated with fatigue crack growth in the base material, and the process would be acceptable. If it was significantly greater then it is hypothesised that the application process may be deficient.

To evaluate this concept we measured the fractal box dimension associated with SPD doublers used on a rib stiffened panel deposited using powders where there was (subsequently) found to be a quality control issue with the powder, i.e. it was found to contain a large proportion of sub 10 micron particles. In this instance the panels had two ten mm wide and 200 mm long SPD doublers located on either side of a centrally located 20 mm long crack, see Fig. 22.

As a result of the poor quality powder one end of each of the two SPD strips delaminated with the locus of the delaminations lying entirely within the SPD, see Figs. 23 and 24. The fractal box dimensions associated with delamination surfaces on each of the two SPD strips, referred to in Figs. 23 and 24 as strips A and B, that delaminated from the structure were measured and the resultant

values are given in Tables 2 and 3. Here we see that in each case the fractal box dimension D was essentially constant at each of the locations measured on each of the two delaminated strips. Furthermore, the value of the fractal box dimension D was approximately 1.5, see Tables 2 and 3. As such the fractal box dimension D associated with these two poor quality SPD's differed significantly from that associated with macro-scopic fatigue crack growth in metals. Thus whilst a great deal more work is needed to validate the hypothesis that D can be used to quantify the quality of the SPD it looks to be worthy of further evaluation. It is interesting to note that prior to these tests a value of $D = 1.5$ had only (previously) been found for very small fatigue cracks [32,34]. A more detailed discussion of the role of the fractal dimension D in describing the nature of the crack tip singularity and in characterising fatigue crack growth is given in [20,34–37].

6. Conclusions and recommendations

The experimental test program has confirmed the potential of SPD doublers to enhance the damage tolerance of structural components. It has also shown how Lock-in themography can be a valuable tool for assessing SPD repairs. We have shown that, as for cracks growing under composite repairs to a cracked metal structure, for the case of a crack growing under a thin SPD patch on an SENT specimen the stress intensity factor can be approximated as being the solution to the SENT specimen subjected to a stress field σ_o which corresponds to the stress in the (base) specimen under the SPD in the absence of a crack. However, this finding may not apply to other problems. Consequently, to assist in the certification process we have also presented weight function solutions for centre cracked panels repaired using SPD.

Acknowledgement

References

[1] Efforts to reduce corrosion on the military equipment and infrastructure of the department of defense, Office of the Secretary of Defense, USA. Department of Defense Report; June 2007.
[2] Karthikeyan, J. 2004. Cold spray technology: International status and USA efforts. ASB Industries. 1-14.
[3] Decker MK, Smith MF. Thermal spray and cold spray analysis of density, porosity, and tensile specimens for use with LIGA applications. SAND2000-0339, Sandia National Laboratories; February 2000.
[4] Sartwell BD, Kestler R, Legg KO, Assink W, Nardi A, Schell J. Validation of HVOF WC/Co, WC/CoCr and Tribaloy 800 thermal spray coatings as a replacement for hard chrome plating on C-2/E-2/P-3 and C-130 propeller hub system components, NRL-PP-99-22-FR-01, Naval Research Laboratory, Washington; May 2003.
[5] Sakaki K. Cold spray process overview and application trends. Mater Sci Forum 2004;449–452:1305–8.
[6] Karthikeyan, J. Development of oxidation resistant coatings on GRCop-84 substrates by cold spray process. NASA-CR 2007-214706; 2007.
[7] Pepi, M. Cold spray technology for repair of magnesium rotorcraft components. NAVAIR corrosion resistant alloy workshop; 8–9, November 2006.
[8] Villafuerte J. Current and future applications of cold spray technology, Recent trends in cold spray technology: Potential applications for repair of military hardware, NATO RTO-MP-AVT-163; 2010. p. 1–14. <ftp://ftp.rta.nato.int>.
[9] Matthews N. Supersonic particle deposition (SPD) cutting edge technology for corrosion protection and damaged metallic component recover In: Proceedings 2010 SDE symposium program "Design Engineering in a SRP Environment". RAAF Williams, Melbourne, Australia; 24–25, March 2010.
[10] Stoltenhoff T. Praxair surface technologies GmbH, Germany, 8th Colloquium, HVOF spraying cold spray, Conference, Erding, Germany; 2009.
[11] Baker AA, Rose LRF, Jones R. Advances in the bonded composite repair of metallic aircraft structure", vol. I and II, Elsevier Applied Science Publishers; 2002. ISBN 0-08-042699-9.
[12] Baker AA, Jones R. Bonded repair of aircraft structure. The Hague: Martinus Nijhoff Publishers; 1988.
[13] Harwood N, Cummings WH. Thermoelastic stress analysis. Bristol: Adam Hilger; 1991.

[14] Dıaz FA, Yates JR, Patterson EA. Some improvements in the analysis of fatigue cracks using thermoelasticity. Int J Fatigue 2004;26:365–76.

[15] Jones R, Pitt S. An experimental evaluation of crack face energy dissipation. Int J Fatigue 2007;28(12):1716–24 (Details on the use of lock-in thermography to measure surface stresses and energy dissipation are given in [13,14].).

[16] N.S. Iyyer, N.E. Dowling, Fatigue growth and closure of short cracks, AFWoAL-TR-89-3008; June 1989.

[17] Newman JC, Wu XR, Venneri SL, Li CG. Small-crack effects in high-strength aluminium alloys, NASA, editor. NASA; 1994.

[18] Jones R. A scientific evaluation of the approximate 2D theories for composite repairs to cracked metallic components, Compos Struct 87(2) (2009) 151–160.

[19] Jones R. Molent L. Critical review of the generalised frost-dugdale approach to crack growth in F/A-18 Hornet structural materials, DSTO-RR-0350; March 2010.

[20] Jones R, Molent L, Pitt S. Crack growth from small flaws. Int J Fatigue 2007;29:658–1667.

[21] Jones R, Barter S, Chen F. Experimental studies into short crack growth. Eng Fail Anal 2011. doi:10.1016/j.engfailanal.2011.03.012.

[22] Zhao ZB, Gillispie BA, Smith JR. Coating deposition by the kinetic spray process. Surf Coat Technol 2006;200:4746–54.

[23] Hussain T, McCartney DG, Shipway PH, Zhang D. Bonding mechanisms in cold spraying: the contributions of metallurgical and mechanical components. J Therm Spray Tech 2008;18(3):364–79.

[24] Pepi M, Cold spray technology for repair of magnesium rotor craft components. In: Proceedings NAVAIR corrosion resistant alloy workshop, 8–9, November 2006.

[25] Rose LRF. A cracked plate repaired with bonded reinforcements. Int J Fract 1982;18:135–44.

[26] Jones R. Numerical analysis and design. In: Baker A, Rose LRF, Jones R, editors. Advances in the bonded composite repair of metallic aircraft structure. Elsevier Applied Science Publishers; 2002. ISBN: 0-08-042699-9.

[27] Jones R. Crack patching: design aspects. In: Baker A, Jones R, editors. Bonded Repair of Aircraft Structure. The Hague: Martinus Nijhoff Publishers; 1988 [chapter 9].

[28] Wang CH, Rose. A crack bridging model for bonded plates subjected to tension and bending. Int J Solids Struct 1999;36:1985–2014.

[29] Jones R, Chiu WK, Marshall IH. Weight functions for composite repairs to rib stiffened panels. Eng Fail Anal 2004;11(1):49–78.

[30] Hart-Smith LJ. Recent expansions in the capabilities of Rose's closed-form analyses for bonded crack-patching. In: Baker A, Rose LRF, Jones R, editors. Elsevier Applied Science Publishers; 2002. ISBN: 0-08-042699-9 [chapter 8].

[31] Mandelbrot BB, Passoja DE, Paullay AJ. Fractal character of fracture surfaces of metals. Nature 1984;308:721–2.

[32] Bouchaud E. Scaling properties of cracks. J Phys Condens Matter 1997;9:4319–44.

[33] Mandelbrot BB. Fractal analysis and synthesis of fracture surface roughness and related forms of complexity and disorder. Int J Fract 2006;138:13–7.

[34] Carpinteri A, Paggi M. A unified fractal approach for the interpretation of the anomalous scaling laws in fatigue and comparison with existing models. Int J Fract 2010;161:41–52.

[35] Spagnoli A. Self-similarity and fractals in the Paris range of fatigue crack growth. Mech Mater 2005;37:519–29.

[36] Saether E, Ta'asan S. A Hierarchical approach to fracture mechanics, NASA/TM-2004-213499.

[37] Carpinteri An, Spagnoli An, Vantadori S, Viappiani D. Influence of the crack morphology on the fatigue crack growth rate: a continuously-kinked crack model based on fractals. Eng Fract Mech 2008;75(3–4):579–89.